RSC Advances

PAPER

View Article Online
View Journal | View Issue

Cite this: *RSC Adv.*, 2017, **7**, 19106

One-pot synthesis of multi-functional magnetite–polysilsesquioxane hybrid nanoparticles for the selective Fe^{3+} and some heavy metal ions adsorption†

Saravanan Nagappan, Hyung Min Ha, Sung Soo Park, Nam-Ju Jo* and Chang-Sik Ha*

Multi-functional magnetite–polysilsesquioxane (PSSQ) hybrid nanoparticles were synthesised in a one-pot approach using ferrous and ferric chlorides and various silane monomers by coprecipitation followed by a surface grafting method. The functional groups, surface properties, and thermal stability of the materials were analyzed using a range of characterisation techniques. Furthermore, the functional magnetic hybrid nanoparticles were used for the adsorption of heavy metal ions. The results suggest that the magnetic PSSQ hybrid nanoparticles have excellent adsorption and selectivity behavior for iron (Fe^{3+}) and some heavy metal ions as individual ions or in mixtures of metal ions. The adsorption kinetics highlighted the excellent adsorption behavior of the functionalised magnetic PSSQ hybrid nanoparticles. On the other hand, the adsorption behavior depends on the type of functional groups present in the materials. These promising and highly desirable magnetic hybrid materials can be used in a wide range of applications.

Received 5th January 2017
Accepted 24th March 2017

DOI: 10.1039/c7ra00159b

rsc.li/rsc-advances

Introduction

Several types of metal and heavy metal ions, such as iron (Fe^{3+}), copper (Cu^{2+}), zinc (Zn^{2+}), lead (Pb^{2+}), cadmium (Cd^{2+}), arsenic (Ar^{3+} and Ar^{5+}), chromium (Cr^{3+}), cobalt (Co^{2+}), and nickel (Ni^{2+}), are commonly found in wastewater from iron and steel manufacturing plants, petroleum refineries, textile mill products, battery and automobile manufacturers, and the paper and pulp industries.[1–4] These metal ions are transferred to the body *via* the consumption of food or water and cause severe damage to health.[5] Some heavy metals are extremely toxic to human beings, even at low concentrations. Iron is an essential element in the human body, which exists mainly in complex forms bound to protein, such as heme compounds (haemoglobin or myoglobin), nonheme compounds (ferritin), flavin-iron enzymes, and heme enzymes.[5–7] On the other hand, excessive amounts of iron in the groundwater gives the water a metallic taste, turbidity, discoloration, odour, stains laundry, *etc.*, as well as iron toxicity.[5–12] According to the world health organisation (WHO), the recommended safe level of iron in drinking water is 0.3 mg L^{-1}.[13,14] Several methods were carried out for the capture of metal ions from water, such as, adsorption, selective separation, ion-exchange, reverse osmosis, filtration, bioremediation, supercritical fluid extraction, *etc.*[5]

Polysilsesquioxane (PSSQ) is a silicon based material which used widely in various applications such as, catalysis, drug delivery, metal ions adsorption, and other applications.[15,16] Recently, functional PSSQ is being used for metal ions adsorption. Burleigh *et al.* first synthesised molecularly imprinted PSSQ by the copolymerisation of 1,2-bis(triethoxysilyl)ethane with metal ion complexes of *N*-[3-(trimethoxysilyl)-propyl]ethylenediamine with cetyltrimethyl ammonium chloride as a surfactant.[17] The material showed excellent adsorption of Cu^{2+}, Ni^{2+}, and Zn^{2+}. On the other hand, bis-amine-bridged PSSQ exhibited excellent adsorption of Cu^{2+} and Pb^{2+} due to the formation of more stable coordination complex between the bis-amine-bridged PSS and metal ions,[18] whereas, the poly(3-mercaptopropylsilsesquioxne) microspheres synthesised by acid and base hydrolysis and the co-condensation of 3-mercaptopropyltrimethoxy silane showed excellent adsorption of Ag^{+} from aqueous solutions.[19] On the other hand, the thiol rich polyhedral oligomeric silsesquioxane showed the adsorption of Hg^{2+}.[20] In general, the sulphur group present in the functional materials showed soft base nature, which prefers to adsorb or bond with soft acid metal ions.[19,21,22] The mercapto functional group also showed the adsorption and complexation behaviour of various other metal ions based on the material nature.

Similar to the PSSQ, the magnetic and magnetic-based functional nanoparticles have potential use in energy, environmental,

Department of Polymer Science and Engineering, Pusan National University, Busan 46241, Republic of Korea. E-mail: csha@pusan.ac.kr; namjujo@pusan.ac.kr; Fax: +82-51-513-7720; Tel: +82-51-510-2407

† Electronic supplementary information (ESI) available: Supplementary text and detailed studies of metal ions adsorptions are available. See DOI: 10.1039/c7ra00159b

and biomedical applications, such as photovoltaics, heavy metal ions adsorption, drug delivery, targeted magnetic resonance imaging (MRI), magnetic hyperthermia, tracking systems for biomolecules, cell separation and labelling, immunoassay, and organic pollutants, such as hazardous organic chemicals and dyes adsorption *etc.*[23–25] The key advantages of magnetic nanoparticles in various applications are the simple synthesis, ease of functionalisation, and magnetic responsive behaviour.[26,27] Furthermore, the materials can be separated easily from solution using a bar magnet and recycled several times without any loss of material. A simple tuning of the surface properties of magnetic-based materials could potentially be used for desirable applications.[28] The combination of magnetic properties with the functional PSSQ can also show excellent adsorption and recycling behaviour of various metal ions.[29–31] Although, the concept of synthesis of magnetic nanoparticles and surface functionalisation of the magnetic nanoparticles are well-known in the literatures, the applications of the magnetic-based materials are emerging continuously in various applications with the modification of synthesis procedure.[32–34] Moreover, most of the surface functionalised magnetic materials were synthesised by two step processes such as synthesis of magnetic nanoparticles followed by the surface functionalisation of the magnetic nanoparticles.

In this study, we synthesised multi-functional magnetic polysilsesquioxane (MFMPSSQ) hybrid nanoparticles in a one-pot approach with range of functional groups, such as mercapto, methyl, and succinic acid groups using various silane precursors. The magnetic nanoparticles was also synthesised for the comparison study. The unique advantages and novelty of the synthesised materials over the other synthesised materials and methods are their simple synthesis of multi-functional groups in one-pot approach, excellent adsorption behaviour, and maintaining good thermal stability of the materials. The adsorption property of the magnetic and functional magnetic nanoparticles were examined using various metal and heavy metal ions, such as Fe^{3+}, Cd^{3+}, Cu^{2+}, Pb^{2+}, and Zn^{2+} in individual or mixed metal ions, and artificial waste water. The adsorption of Fe^{3+} by the mercapto functional PSS or other types of mercapto based multi-functional materials rarely occurred. To the best of the authors' knowledge, this is the first report of the adsorption of heavy metal ions, particularly with the maximum and high selective adsorption of Fe^{3+} ions using multi-functional (mercapto or succinic acid) magnetic PSSQ. The metal ions adsorption is based on the surface functional groups grafted to the magnetite nanoparticles.

Materials and methods

Materials

The materials for this work include ferric(III) chloride hexahydrate ($FeCl_3 \cdot 6H_2O$, ≥98%), ferrous(II) chloride tetrahydrate ($FeCl_2 \cdot 4H_2O$, ≥99%), (3-mercaptopropyl)trimethoxy silane (MPTMS, ≥80%), (3-mercaptopropyl)methyldimethoxysilane (MPMDMS, ≥98%), triethoxysilylpropyl succinic anhydride (TESPSA, ≥95%), iron(III) nitrate nonahydrate ($Fe(NO_3)_2 \cdot 9H_2O$, 98%), cadmium nitrate tetrahydrate ($Cd(NO_3)_2 \cdot 4H_2O$, 98%), copper(II) nitrate trihydrate ($Cu(NO_3)_2 \cdot 3H_2O$, 98–103%), lead(II) nitrate ($Pb(NO_3)_2$, ≥99%), zinc nitrate hexahydrate ($Zn(NO_3)_2 \cdot 6H_2O$, 98%), manganese(II) nitrate tetrahydrate ($Mn(NO_3)_2 \cdot 4H_2O$, 97%), cobalt(II) nitrate hexahydrate ($Co(NO_3)_2 \cdot 6H_2O$, 98%), lithium nitrate ($LiNO_3$, 98%), nickel(II) sulphate hexahydrate ($Ni(SO_4)_2 \cdot 6H_2O$, 98.5%), aluminium nitrate nonahydrate ($Al(NO_3)_2 \cdot 9H_2O$, 98%), magnesium nitrate hexahydrate ($Mg(NO_3)_2 \cdot 6H_2O$, 99%), calcium nitrate tetrahydrate ($Ca(NO_3)_2 \cdot 4H_2O$, 98%), and sodium nitrate ($NaNO_3$, 99%). All chemicals were purchased from Sigma-Aldrich. The ammonia (NH_3, 30%) solution and sodium hydroxide (NaOH, 97%) were obtained from Junsei Chem. Pvt. Ltd. All chemicals were used without further purification.

One-pot synthesis of multi-functional magnetite polysilsesquioxane hybrid nanoparticles

Magnetic nanoparticles (MNPs) suspension was synthesised by dissolving $FeCl_3 \cdot 6H_2O$ (0.01 M, 2.7 g) and $FeCl_2 \cdot 4H_2O$ (0.005 M, 1.0 g) at a 2 : 1 ratio in 50 mL of water under a N_2 atmosphere. The solution was stirred for a few minutes followed by the addition of 50 mL of an aqueous ammonia solution (1 M).[35,36] A black precipitate was obtained immediately by the addition of aqueous ammonia and stirring was continued for 15 min. For the comparison study, the MNPs precipitate was decanted by a bar magnet, filtered, washed with excess amounts of water and ethanol, and dried at 150 °C for 12 h in a vacuum oven and named as FeS0 (Scheme 1). On the other hand, the *in situ* surface medication was carried out in one-pot by adding anhydrous ethanol (50 mL) to the MNPs suspension (before washing) followed by the addition of CTAB (0.5 mM, 0.18 g), and MPTMS (0.005 M, 0.97 g) to the suspension and stirred continuously for 6 h in N_2 atmosphere. MPTMS (0.005 M, 0.97 g) was then added to the solution and stirred for another 12 h (FeS1). The reaction was also carried out for a comparison study with the addition of other silane precursors in the second stage (12 h stirring), such as MPMDMS (0.005 M, 0.90 g, FeS2), or TESPSA (0.005 M, 1.55 g, FeS3) instead of MPTMS (0.005 M, 0.97 g). The precipitates were decanted by a bar magnet, filtered, and washed with an excess of water and ethanol, and dried at 150 °C for 12 h in a vacuum oven. CTAB was removed from the materials by washing the samples with an ethanol/acetic acid (0.1 mol)/acetone solution. Succinic anhydride (SA) in TESPSA was hydrolyzed by the addition of 50.0/1.0 mL of a water/acidic acid solution followed by shaking at 150 rpm for 30 min, filtering, washing with ethanol, and drying overnight at 60 °C in an vacuum oven (Schemes 1 and 2). The synthesised magnetic PSSQ hybrid nanoparticles showed a random structure of functional silsequioxane networks attached to the magnetic nanoparticles surface. The nanoparticles for Fe_3O_4, the mercaptopropyl magnetic PSSQ, methyl-mercaptopropyl magnetic PSSQ, and succinic acid-mercaptopropyl magnetic PSSQ hybrid nanoparticles were called FeSo, FeS1, FeS2, and FeS3, respectively, according to the functional silsequioxane networks.

Adsorption of metal ions

Metal ions adsorption was carried out by preparing individual solutions of various metal ions, such as Cd^{2+}, Cu^{2+}, Pb^{2+}, and Zn^{2+}, at fixed concentration (5 mM in 1 L) and the pH of the

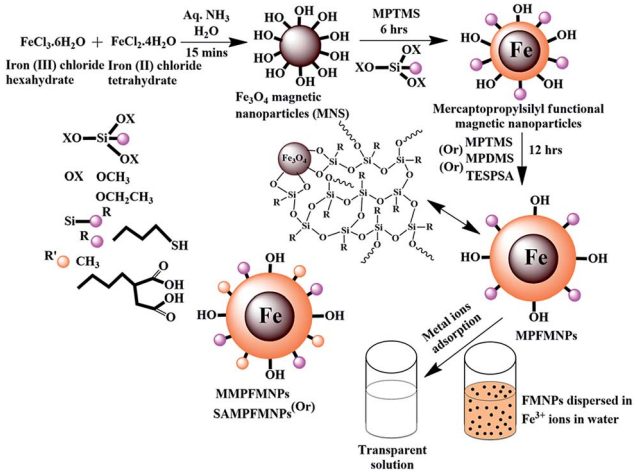

Scheme 1 One-pot synthesis of functional polysilsesquioxane (PSSQ) magnetite hybrid nanoparticles.

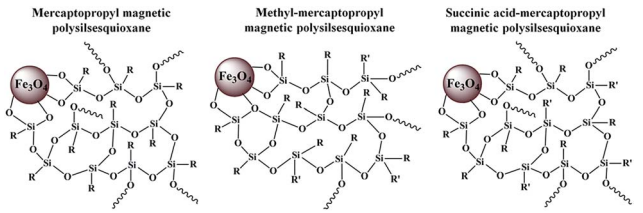

Scheme 2 Schematic diagram of functional PSSQ magnetite hybrid nanoparticles.

solutions were adjusted to pH 6 using sodium hydroxide (NaOH) and hydrochloride (HCl) solutions. The metal ions solutions (5 mL) were taken in a 10 mL glass vial capped with a plastic screw cap followed by the addition of adsorbent (20 mg) and agitated constantly at 180 rpm and 298 K for 24 h. The iron (Fe^{3+}) solution was prepared using $FeCl_3 \cdot 6H_2O$ at pH 3 and the extent of metal ion adsorption under the above conditions was checked. Furthermore, a mixed metal ions solution of five metals (Fe^{3+}, Cd^{2+}, Cu^{2+}, Pb^{2+}, and Zn^{2+}, each 5 mM) was also prepared and the pH of the solution was adjusted to pH 3 according to the above experimental procedure.

Preparation of artificial waste water

The artificial waste water was prepared by mixing the following ten elements: $Mn(NO_3)_2 \cdot 4H_2O$, $Co(NO_3)_2 \cdot 6H_2O$, $LiNO_3$, $Fe(NO_3)_2 \cdot 9H_2O$, $Ni(SO_4)_2 \cdot 6H_2O$, $Al(NO_3)_2 \cdot 9H_2O$, $Mg(NO_3)_2 \cdot 6H_2O$, $Zn(NO_3)_2 \cdot 6H_2O$, $Ca(NO_3)_2 \cdot 4H_2O$, and $NaNO_3$ at concentrations of 5 mM for each element. It should be noted that the concentration of the prepared solution is quite higher than the natural or wastewater streams. We used such concentrated solution, however, to prove the excellent adsorption behaviour of our materials more clearly. The pH of the solution was adjusted to pH ~2 to 3 and a similar experiment procedure to that mentioned above was followed. Table S1† lists the chemical compositions of the metal ions used to prepare 5 mM of artificial waste water in 1 L. The experiment was also carried at various time intervals with various amounts of adsorbents. The recyclability test was carried by washing the adsorbed materials with double deionised water and ethanol a few times and drying at 60 °C for 1 h prior to use in the next cycle using similar experimental procedures. The amount of metal ion adsorption at a give time (q_t) and the percentage removal efficiency (R) were calculated using the following equations:

$$q_t = (C_o - C_t)V/W \quad (1)$$

$$R\ (\%) = (C_o - C_t)/C_o \times 100 \quad (2)$$

where C_o and C_t represent the initial and final concentrations (mg L^{-1}) of metal ions at a given time (t). V and W denote the volume (mL) of the solution and weight of the adsorbent (mg) used for adsorption, respectively. The adsorption experiment was repeated for three times and averaged the obtained results. The adsorption capacity was calculated further using 1 g of adsorbent per litre of metal ion solution. The selectivity (in percentage) of each metal ions in the mixed metal ions and in the artificial waste water were calculated from the below formula.

$$\text{Selectivity}\ (\%) = (q_e/Sq) \times 100 \quad (3)$$

where q_e is the adsorption capacity of metal ions at equilibrium and Sq_e is the sum of the adsorption capacity of all the metal ions at equilibrium.

Characterisation

The surface functional groups present in the magnetic and functionalised magnetic nanoparticles were analyzed by Fourier transform infrared spectroscopy (FTIR, JASCO (FTIR-4100)) at a scanning range over 400–4000 cm^{-1}. Pellet samples were prepared using potassium bromide (KBr) prior to analysis. The surface morphology the samples were examined by high resolution scanning electron microscopy (HRSEM, Hitachi S-4800) and high resolution transmission electron microscopy (HRTEM, JEM 2011 at 200 kV). The HRSEM samples were prepared by loading the powders on carbon tape followed by coating with osmium tetraoxide (Hatfield, PA-19440). The HRTEM samples were prepared by dispersing the samples in ethanol followed by loading the samples on a copper grid and drying before the measurement. The surface area, pore volume and pore size distributions of the functionalised magnetic nanoparticles were analyzed by nitrogen adsorption and desorption isotherms (Micromeritics ASAP 2020 V3.04 G) and calculated using Brunauer–Emmett–Teller (BET) and Barrett–Joyner–Halenda (BJH) methods. The structural properties of the materials were measured by X-ray diffraction (XRD, Miniflex goniometer using CuKα irradiation) at the scanning range of 1.2–80.0° 2θ with a 0.02° 2θ scanning speed. The thermal stability of the materials was checked in a nitrogen atmosphere at a heating rate of 10 min^{-1} by thermogravimetric analysis (TGA, Q50 V6.2, Build 187, TA instruments, U.S.). Furthermore the magnetic property of the synthesised materials was

analysed by a superconducting quantum interference device (SQUID) magnetometer (Quantum design, MPMS XL). The adsorption of metal ions was monitored by inductive coupled plasma optical emission spectroscopy (ICP-OES, Agilent 5100).

Results and discussion

Fig. 1a shows the surface functionality of the synthesised Fe_3O_4 magnetic nanoparticles. The peak at 580 cm^{-1} was assigned to the presence of a Fe–O bond in the Fe_3O_4 magnetic nanoparticles.[37] Fig. 1b presents the MPTMS functionalised magnetic PSSQ nanoparticles after removing the surfactant. The main peaks of Si–O–Si, Si–CH_2, C–H asymmetric and symmetric stretching and bending vibrations, S–H, Si–OH, and Fe–O–Si bonds were observed at 1130, 1080, 800, 1260, 2950, 2880, 2560, 910, and 602 cm^{-1}, respectively.[38,39] The change in the Fe–O bond from 576 cm^{-1} to 602 cm^{-1} was due to the formation of Fe–O–Si bond. Similar results were obtained by a surface treatment with other silane precursors, such as MPMDMS and succinic acid (SA) (Fig. 1c and d). The magnetic nanoparticles synthesised by the coprecipitation method showed a spherical shape with very small nanoparticles (Fig. 2a). The HRTEM image also clearly showed the spherical shape of the magnetic nanoparticles (~11.3 nm, Fig. 3a). Fig. 2(b–d) and 3(b–d) show the surface morphology of the functionalised magnetic PSSQ nanoparticles with MPTMS, MPMDMS, and TESPSA. The functionalised magnetic nanoparticles aggregated and interconnected and formed network structures, as shown in Fig. 2(b–d) and 3(b–d). The Fe_3O_4 magnetic nanoparticles synthesised by the coprecipitation method showed a porous structure with a type IV hysteresis loop (Fig. 4A(a)). The adsorption and desorption isotherm curve had mesoporous structures of the synthesised Fe_3O_4 magnetic nanoparticles. The porous structure may be due to of the formation of mesoporous voids formed by the aggregation of magnetic nanoparticles due to magnetic–magnetic dipole interactions. The surface area, pore volume and pore size distributions values were 119 $m^2\ g^{-1}$, 0.31 $cm^3\ g^{-1}$ and 13.1 nm for the magnetic nanoparticles (Fig. 4A(a) and B(a), and Table 1). On the other hand, reduced surface areas, pore volumes, and pore size distributions were occurred by treating with various functional groups as compared to the pristine magnetic nanoparticles.

The MPTMS functionalised PSSQ magnetic nanoparticles also exhibited a porous structure with surface area, pore volume, and pore size distributions of 38 $m^2\ g^{-1}$, 0.05 $cm^3\ g^{-1}$, and 21.6 nm (Fig. 4A(b) and B(b), and Table 1), whereas, the above values were altered after modification of the magnetic nanoparticles with MPMDMS, and TESPSA (Fig. 4A(c and d) and B(c and d), and Table 1). This might be due to the different chemical nature of the surface functional groups used for the synthesis. The reductions in the surface areas, pore volumes,

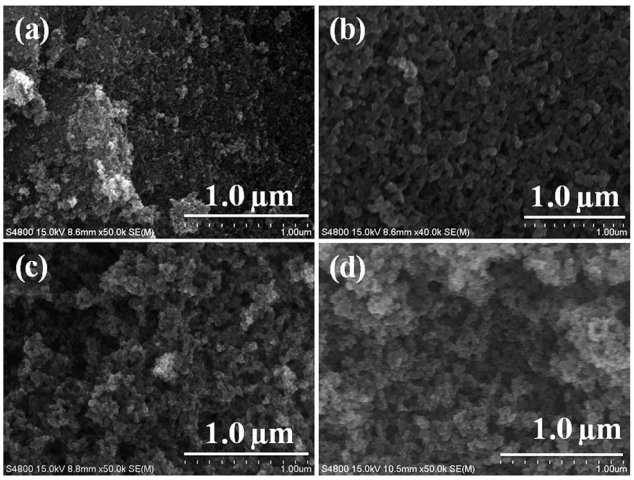

Fig. 2 HR-SEM images of (a) Fe_3O_4 (FeS0), (b) mercaptopropyl (FeS1), (c) methyl-mercaptopropyl (FeS2), and (d) succinic acid-mercaptopropyl (FeS3) magnetic PSSQ hybrid nanoparticles.

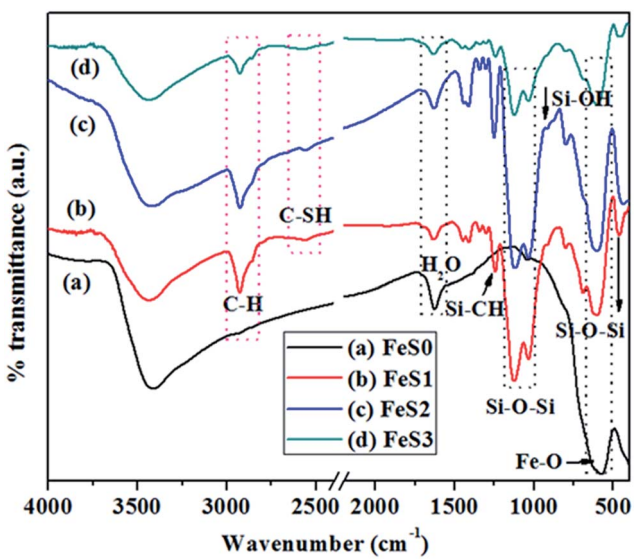

Fig. 1 FTIR spectra of (a) Fe_3O_4 (FeS0), (b) mercaptopropyl (FeS1), (c) methyl-mercaptopropyl (FeS2), and (d) succinic acid-mercaptopropyl (FeS3) magnetic PSSQ hybrid nanoparticles.

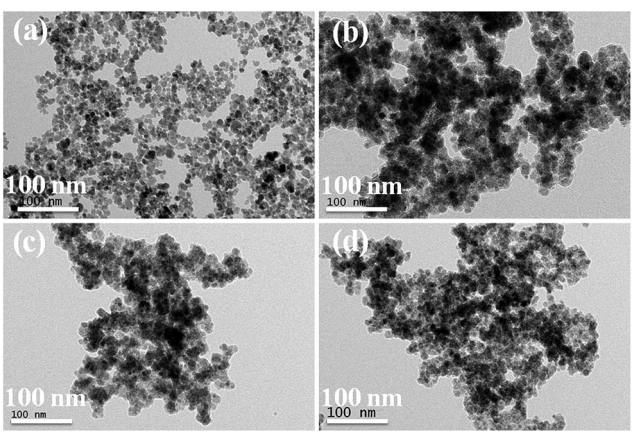

Fig. 3 HR-TEM images of (a) Fe_3O_4 (FeS0), (b) mercaptopropyl (FeS1), (c) methyl-mercaptopropyl (FeS2), and (d) succinic acid-mercaptopropyl (FeS3) magnetic PSSQ hybrid nanoparticles.

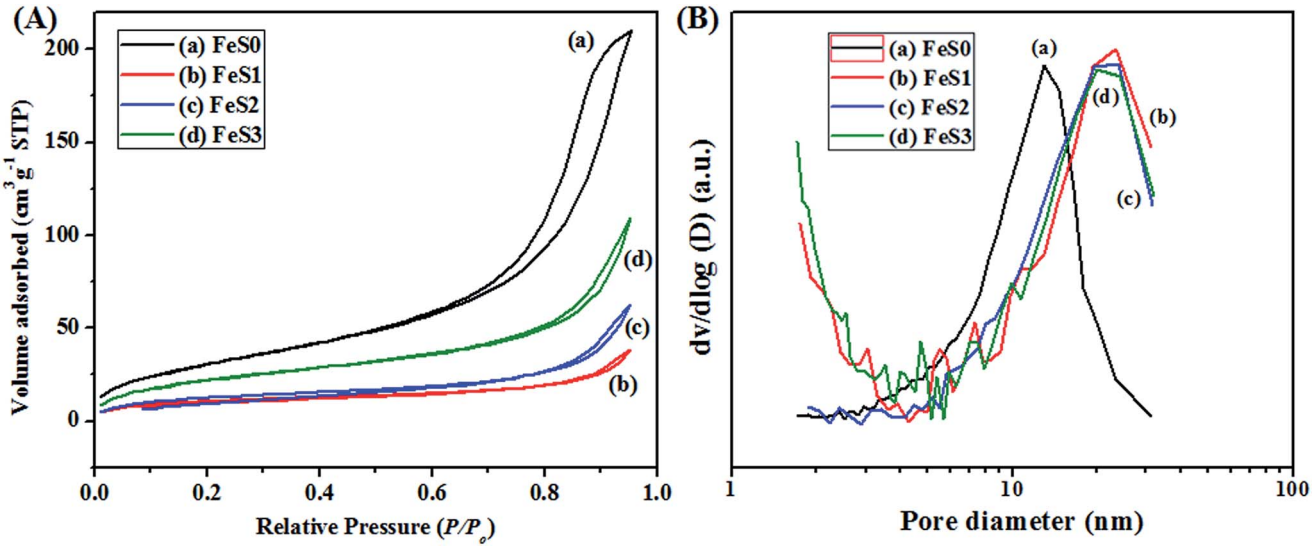

Fig. 4 N_2 adsorption/desorption isotherms (A) and pore size distribution (B) of (a) Fe_3O_4 (FeS0), (b) mercaptopropyl (FeS1), (c) methyl-mercaptopropyl (FeS2), and (d) succinic acid-mercaptopropyl (FeS3) magnetic PSSQ hybrid nanoparticles.

Table 1 BET surface areas, pore volumes and BJH pore diameters, and the thermal decomposition and weight loss values of magnetite and functionalised magnetic PSSQ hybrid nanoparticles

Name	BET surface area ($m^2\ g^{-1}$)	Total pore vol. ($cm^3\ g^{-1}$)	BJH pore dia. (nm)	T_{d5}[a] (°C)	T_{d10}[b] (°C)	Res. wt at 800 °C (%)
FeS0	119	0.31	13.1	329	—	91.9
FeS1	38	0.05	21.6	308	376	72.1
FeS2	45	0.09	21.6	297	373	76.4
FeS3	83	0.15	18.7	289	378	77.0

[a] The temperature at which 5% of weight loss is observed. [b] The temperature at which 10% of weight loss is observed.

and pore size distributions of the functionalised magnetic nanoparticles were due to the formation of additional functional groups which block the porous structure of the magnetic nanoparticles and reduce the above properties. The XRD pattern of the Fe_3O_4 magnetic nanoparticles in Fig. 5a indicates the crystalline nature. The peaks at (311), (220), (400), (422), (511), and (440) planes confirmed the inverse spinel structure of the Fe_3O_4 magnetic nanoparticles (Fig. 5a).[37] The functionalised magnetic nanoparticles also showed similar crystalline peaks (Fig. 5(b–d)). The results suggest that the crystalline structure of the Fe_3O_4 magnetic nanoparticles was maintained after the functionalisation of nanoparticles with various silane precursors.

The thermal stability of the synthesised and functionalised magnetic nanoparticles were checked (Fig. 6A). The magnetic nanoparticles showed two major decomposition peaks (Fig. 6A(a)), which were attributed to the removal of hydrogen bonded water at the first stage (~170 °C) and trapped water molecules from the lattice cell at the second stage (~350 °C). The Fe_3O_4 magnetic nanoparticles showed approximately 92% residual mass after heating the sample to 800 °C. The higher residual mass is due to the formation of Fe–O bonds through the loss of water moieties after heating the sample to more than 560 °C and showed excellent thermally stability of the Fe_3O_4 magnetic nanoparticles (Table 1).[37] The thermal stability of MPTMS functionalised magnetic PSSQ nanoparticles showed improved initial degradation properties from ~160 °C to ~260 °C due to the presence of a long alkyl chain and the higher boiling point (213–215 °C) of MPTMS on the surface of the magnetic nanoparticles, which delayed the initial degradation of water moieties and organic alkyl chains (Fig. 6A(b)). Similar results were obtained for other functionalised PSSQ obtained from MPMDMS and TESPSA (Fig. 6A(c and d)). The 5 and 10 wt% losses suggest that the functionalised materials decompose the alkyl chains at temperatures of 280 °C to ~380 °C. This decomposition behaviour may vary according to the type of functional silanes used for the modification of magnetic nanoparticles. Moreover, the decomposition results at this stage are not uniform due the overlap of functional groups and the functionalisation carried out in one-pot approaches. On the other hand, the final residual mass obtained at an ~800 °C annealing temperature clearly showed 19.8% MPTMS capped on the Fe_3O_4 magnetic nanoparticles (Table 1), whereas the functional PSSQ magnetic nanoparticles synthesised from MPMDMS and TESPSA showed a small decrease in encapsulation by the one-pot approach. The difference in encapsulation

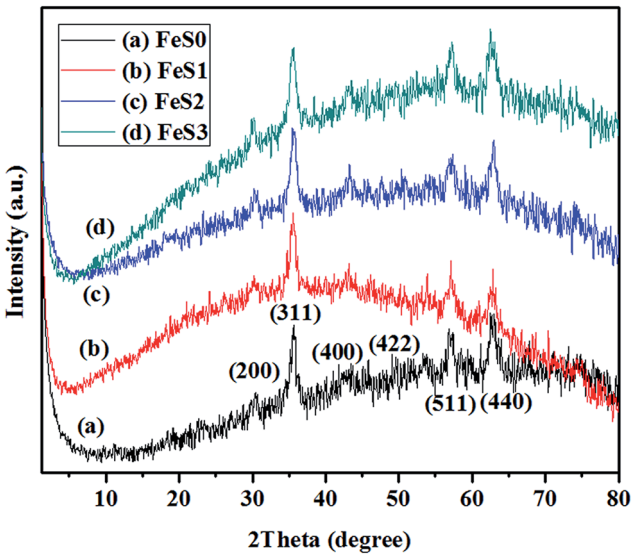

Fig. 5 XRD patterns of (a) Fe_3O_4 (FeS0), (b) mercaptopropyl (FeS1), (c) methyl-mercaptopropyl (FeS2), and (d) succinic acid-mercaptopropyl (FeS3) magnetic PSSQ hybrid nanoparticles.

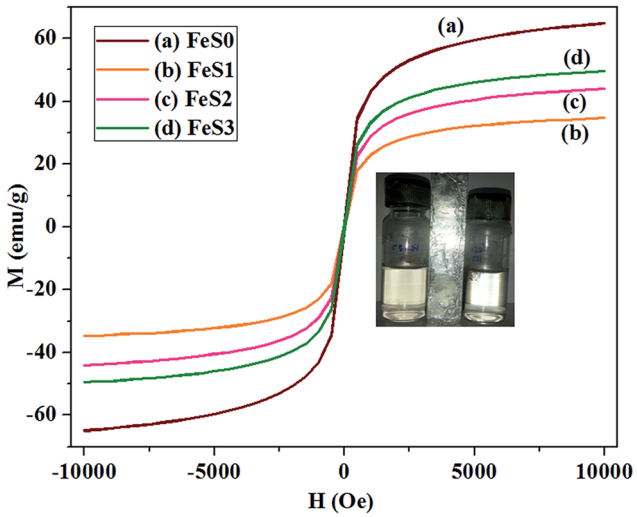

Fig. 7 Magnetic susceptibility (M) of (a) Fe_3O_4 (FeS0), (b) mercaptopropyl (FeS1), (c) methyl-mercaptopropyl (FeS2), and (d) succinic acid-mercaptopropyl (FeS3) magnetic PSSQ hybrid nanoparticles. The inset image shows the magnetic properties of the materials in the water (left (FeS1) and right (FeS3)).

results may be due to the dissimilarity between the initial MPTMS modification followed by the use of other silanes and to the presence of hydrophobic and hydrophilic functional groups in the mixture solution, which may reduce the encapsulation efficiency (Fig. 6A and Table 1). DTA also confirmed the above properties (Fig. 6B).

The magnetic susceptibility (M) of the Fe_3O_4 and functional PSSQ magnetic nanoparticles obtained from MPTMS, MPMDMS, and TESPSA was analysed further (Fig. 7). The Fe_3O_4 magnetic nanoparticles obtained from the coprecipitation method showed a very strong magnetic hysteresis loop (65.7 emu g^{-1}) with superparamagnetic properties. This is due to the formation of a very small nanoparticle size (~10.0–12.0 nm) by the coprecipitation method. The nanoparticles can interact effectively with each of the magnetic nanoparticles by magnetic dipole–dipole interactions and showed a higher saturation of magnetisation. The functionalised PSSQ nanoparticles obtained from MPTMS, MPMDMS and TEPSA showed the partially reduced saturation of magnetisation. The maximum magnetisation for MPTMS, MPMDMS and TEPSA occurred at 34.7, 44.0 and 49.5 emu g^{-1} (Fig. 7). The reduced saturation of magnetisation was attributed to the surface capping of functional groups on the surface of the magnetic nanoparticles and the surface spin effect on Fe_3O_4 by functionalisation. The inset in Fig. 7 shows the magnetic properties of the materials in the water (left (FeS1) and right (FeS3)).

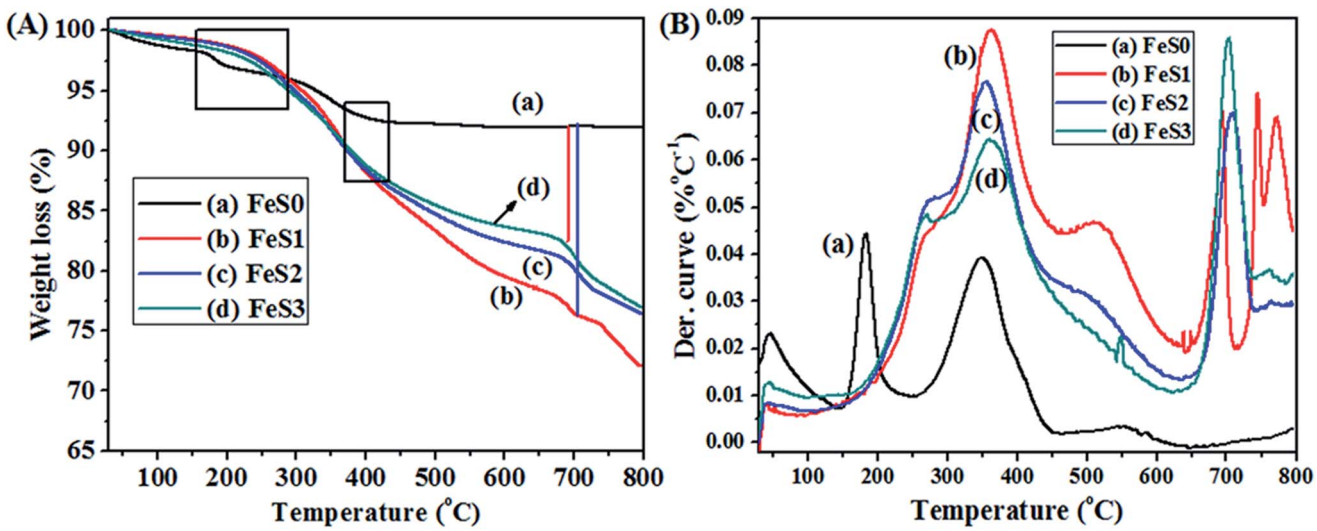

Fig. 6 TGA (A), and DTA curves (B) of (a) Fe_3O_4 (FeS0), (b) mercaptopropyl (FeS1), (c) methyl-mercaptopropyl (FeS2), and (d) succinic acid-mercaptopropyl (FeS3) magnetic PSSQ hybrid nanoparticles.

Fig. 8 shows the individual metal ion adsorption by the magnetic and functionalised magnetic hybrids. The magnetic nanoparticles (FeS0) adsorbed heavy metal ions, such as Cd^{2+}, Cu^{2+}, Pb^{2+}, and Zn^{2+} (5.2, 30.0, 66.1, 13.3 mg g^{-1}, respectively) with a removal efficiency of (1.2, 16.0, 8.9, and 5.8%, respectively) (Fig. 8A and B), whereas, the this may show the adsorption and removal efficiency of 68.4 mg g^{-1} and 34.2%, respectively, for Fe^{3+} ions (Fig. 8A and B). The adsorption efficiency of the magnetite nanoparticles for heavy metal ions was in the order of $Fe^{3+} > Cu^{2+} > Pb^{2+} > Zn^{2+} > Cd^{2+}$. The adsorption of these metal ions occurs mainly by the physico-chemical interactions or likely by electrostatic attractions. Similar phenomena was illustrated for the adsorption of Pb^{2+}, Zn^{2+}, Cu^{2+}, Mn^{2+}, As^{3+}, As^{5+}, and Cr^{6+} by the magnetite and maghemite nanoparticles.[40–42] The functionalisation of magnetite nanoparticles with the mercaptopropyl functional PSSQ (FeS1) structure showed enhanced adsorption behaviour and a higher removal efficiency of heavy metal ions ($Fe^{3+} > Cu^{2+} > Zn^{2+} > Pb^{2+} > Cd^{2+}$) as compared with than that of the pristine magnetite nanoparticles (Fig. 8A and B). The adsorption behaviour for Fe^{3+}, Cd^{2+} and Zn^{2+} was increased approximately three times with small changes observed for Cu^{2+} and Pb^{2+}. The enhanced adsorption of heavy metal ions was attributed to the formation of covalent bonds between the thiol functional groups with metal ions and the presence of a porous network structure of PSSQ magnetic nanoparticles.[43]

The thiol functional groups were highly active to various heavy metal ions, such as Hg^{+}, Au^{+}, Ag^{+}, Pb^{2+}, Cd^{2+}, Cu^{2+}, Ni^{2+}, and Zn^{2+}, through covalent bonds or Lewis acid–base interactions.[43–46] This preliminary study found the new highlight of the adsorption of Fe^{3+} ions by the mercaptopropyl functional magnetic PSSQ hybrid with the maximum adsorption of 174.4 mg per 1 g of adsorbent with a removal efficiency of 87.5% in 24 h (Fig. 8A and B). On the other hand, metal ions adsorption was reduced dramatically by simple tuning of the surface property of the mercapto functionalised magnetic nanoparticles (FeS2) with the introduction of hydrophobic methyl functional group in the mercaptopropyl functional PSSQ surface (Fig. 8A and B). This might be due to the hydrophobic effect of the functionalised magnetic nanoparticles, which repels the metal ions and prevents the formation of a strong covalent bond between the surface functional group and metal ions.

In general, the succinic acid functional groups showed excellent adsorption to Cu^{2+}, Cd^{2+}, Pb^{2+}, and Zn^{2+}.[47–49] The introduction of succinic acid functional groups with the mercaptopropyl group in the magnetic PSSQ hybrid (FeS3) showed excellent adsorption of Fe^{3+}, Pb^{2+}, Cu^{2+}, and Cd^{2+}, whereas, Cu^{2+}, Cd^{2+} and Pb^{2+} adsorption were improved with slightly lower Fe^{3+} and Zn^{2+} adsorption by the succinic acid-mercaptopropyl functionalised magnetic PSSQ hybrid than the mercaptopropyl functionalised magnetic PSSQ hybrid (Fig. 8A and B). The

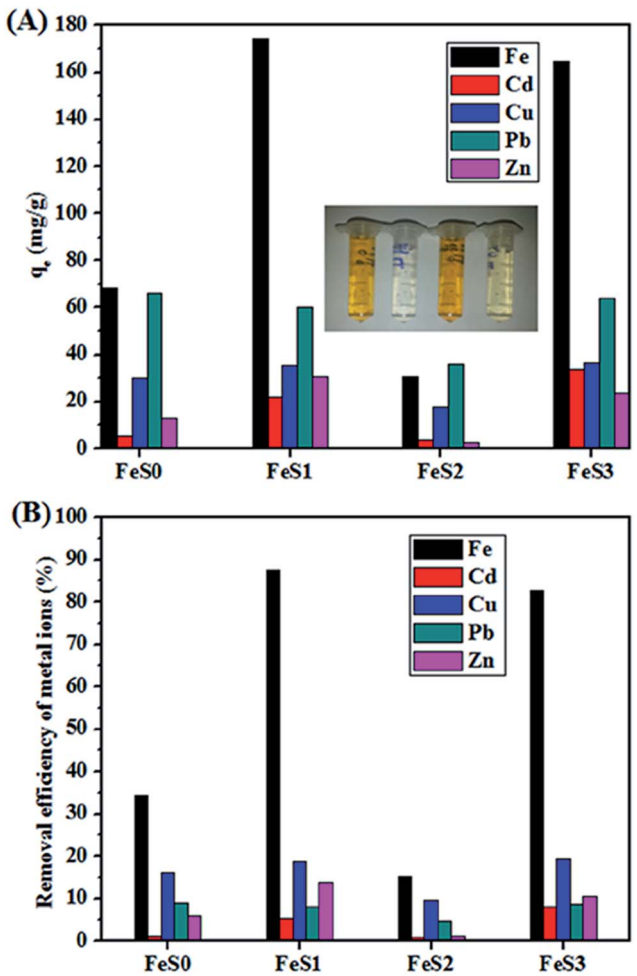

Fig. 8 ICP-OES results of the adsorption capacity (A) and percentage removal efficiency (B) (in 24 h) of individual metal ions on the Fe_3O_4 (FeS0), mercaptopropyl (FeS1), methyl-mercaptopropyl (FeS2), and succinic acid-mercaptopropyl (FeS3) magnetic PSSQ hybrid nanoparticles. The inset image shows the colour differences of the Fe^{3+} ions solution after adsorption (from left to right-FeS0, FeS1, FeS2, and FeS3).

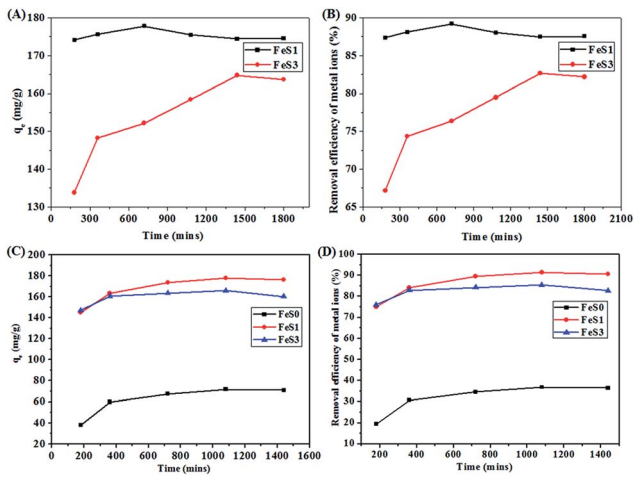

Fig. 9 ICP-OES results of the effect of the contact time on the adsorption capacity (A) and percentage removal efficiency (B) of Fe^{3+} ions on the mercaptopropyl (FeS1) and succinic acid-mercaptopropyl (FeS3) magnetic PSSQ hybrid nanoparticles. Effect of the contact time on the adsorption capacity (C) and percentage removal efficiency (D) of Fe^{3+} ions from the mixed metal ions by the Fe_3O_4 (FeS0), mercaptopropyl (FeS1) and succinic acid-mercaptopropyl (FeS3) magnetic PSSQ hybrid nanoparticles.

increase in metal ion adsorption is due to the formation of a strong covalent bond between the multi-functional groups on the PSSQ surface.[50] The presence of multi-functional group in the magnetic PSSQ hybrid showed the unique adsorption of Fe^{3+} and other metals ions in the individual solutions. Furthermore, the adsorption behaviors of Fe^{3+} by the mercaptopropyl and succinic acid mercaptopropyl magnetic PSSQ hybrids were analysed at various adsorptions times (Fig. 9A and B).

The kinetics of adsorption suggests that the mercaptopropyl functionalised magnetic PSSQ hybrid (FeS1) showed much faster adsorption of Fe^{3+} than the succinic acid-mercaptopropyl magnetic PSSQ hybrid nanoparticles (FeS3) in the initial few hours (within 3 h), which reached equilibrium within 12 h. The yellowish color of the Fe^{3+} solution becomes transparent by shaking the solution at or over the equilibrium time (inset image in Fig. 8A). The maximum adsorption (177.8 mg g^{-1}) and removal efficiency (89.2%) of Fe^{3+} was achieved within 12 h and was reduced slightly by further increasing the adsorption time and saturated at 24 h of shaking time (FeS1, 174.4 mg g^{-1} (87.5%) in 24 h, Fig. 9A and B and Table 2). Similarly, the succinic acid-mercaptopropyl group functionalised magnetic PSSQ hybrid also showed good adsorption of Fe^{3+} ions at the initial time with further increases in adsorption with increasing adsorption time. The materials achieved the maximum adsorption at 24 h with an adsorption capacity and removal efficiency of 164.8 mg g^{-1} and 82.7%, respectively (Fig. 9A and B and Table 2). The adsorption behaviour was reduced partially by further increasing the adsorption time (Fig. 9A and B). The above samples also showed similar adsorption capacity of Fe^{3+} metal ions at pH 3 in 24 h up to 3 cycles (ESI, Fig. S1†). The synthesized materials are also stable for 24 h in water or buffer solutions of three different pHs (pH = 4.0, 5.5, 7.0), as shown in Fig. S2 (in ESI†), due to the stable polysilsequioxane structure of the surface modified magnetic nanoparticles. Moreover, the excellent recycling ability of the materials confirms the stable surface property.

Fig. 9C and D presents the adsorption capacity of Fe^{3+} ions from the mixed metal ions by the magnetite, mercaptopropyl and succinic acid-mercaptopropyl functionalised magnetic PSSQ hybrids. The magnetite and functionalised magnetic PSSQ hybrids clearly adsorbed various metal ions from the mixed metal ions solutions (Fig. 9C and D, and Table S2†). On the other hand, the functionalised magnetic PSSQ hybrids also showed excellent adsorption and selectivity for Fe^{3+} from the mixed metal ions than the magnetite nanoparticles (Fig. 9C and D, Fig. S3–S5 (in ESI†), and Table 2). These results also suggest

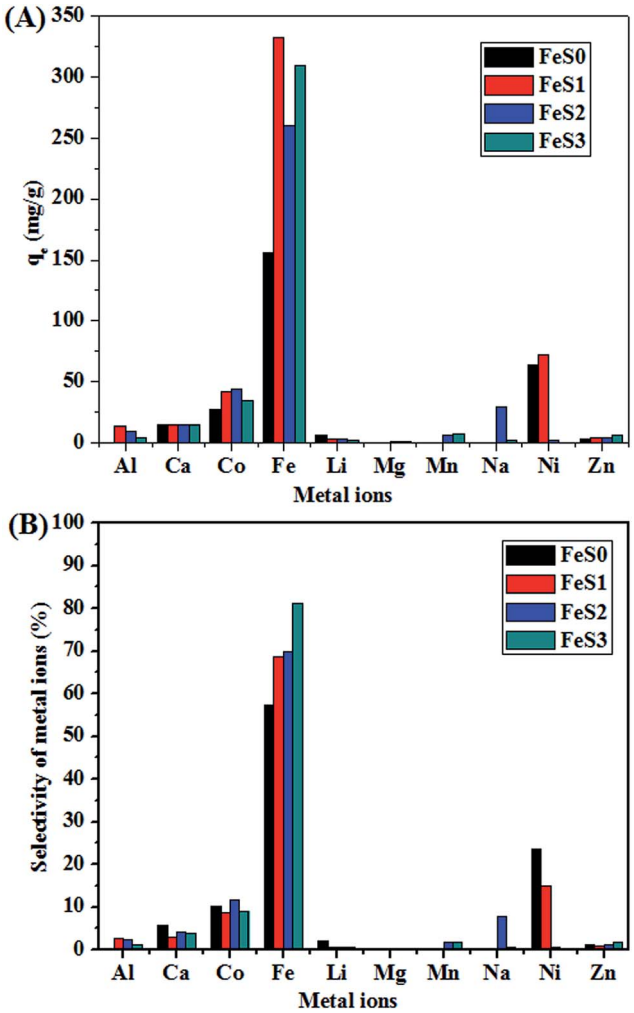

Fig. 10 ICP-OES results of the adsorption capacity (A) and selectivity of metal ions (B) from the artificial waste water on the Fe_3O_4 (FeS0), mercaptopropyl (FeS1), methyl-mercaptopropyl (FeS2), and succinic acid-mercaptopropyl (FeS3) magnetic PSSQ hybrid nanoparticles.

Table 2 Pseudo second-order kinetic parameters for the adsorption of Fe^{3+} ions in the individual (Ind.) or mixed (mix.) metal ions onto various adsorbents[a]

	Pseudo second order				
Adsorbent	q_e (mg g^{-1}) (exp.)	q_e (mg g^{-1}) (theo.)	$k_{2,ads}$ (g mg^{-1} min)	h (mg g^{-1} min)	R^2
FeS1 (Ind. Met)	177.8	174.2	0.0014	36.42	0.9999
FeS3 (Ind. Met)	164.8	168.9	0.0001	2.850	0.9992
FeS0 (Mix. Met)	71.74	80.13	0.0001	0.640	0.9933
FeS1 (Mix. Met)	177.9	182.5	0.0001	3.330	0.9996
FeS3 (Mix. Met)	165.8	163.4	0.0008	21.40	0.9986

[a] q_e amount of adsorption at equilibrium, k_2-equilibrium rate constant, h-initial sorption rate, R-correlation coefficient, (exp. – experimental, theo. – theoretical).

that the maximum amount of Fe^{3+} adsorption were increased to some extent in the mixed metal ions solutions (71.64 mg g^{-1} for FeS0, 177.9 mg g^{-1} for FeS1, and 165.8 mg g^{-1} for FeS3) than the individual metal ions solutions (68.4 mg g^{-1} for FeS0, 177.8 mg g^{-1} for FeS1, and 164.8 mg g^{-1} for FeS3) (Table 2).

The adsorption behaviour and selectivity of the magnetite, and functionalised magnetic PSSQ hybrids in artificial waste water was also checked (Fig. 10A and B). The magnetic and functionalised magnetic PSSQ hybrids also showed excellent adsorption capacity (155.3 mg g^{-1} for FeS0, 332.1 mg g^{-1} for FeS1, 260.8 mg g^{-1} for FeS2, and 309.6 mg g^{-1} for FeS3) and selectivity to Fe^{3+} compared to the other metal ions (Fig. 10A and B). We also compared our materials with some of the materials used for the adsorption of Fe^{3+} ions and summarised in Table 3.[50–59]

To the best of author's knowledge, this is first report of excellent adsorption and selectivity of Fe^{3+} ions in water, mixed metal ions solutions, and artificial waste water by multi-functional magnetic PSSQ hybrid materials as compared with various functional (such as mercapto, amine, carboxylic, and other functional groups) materials. The kinetics of Fe^{3+} adsorption was analysed in detail using pseudo-first order and pseudo-second order models, as described in ESI.† The adsorption kinetics of Fe^{3+} ions fitted the pseudo-second order model well. Table 2 lists the kinetic parameters for the pseudo-second order model. The adsorption kinetic study also proved the pseudo second order adsorption of Fe^{3+} ions from the individual or mixed metal ions on the functionalised magnetic PSSQ hybrids (ESI,† Fig. S6 and S7, Tables 2, and S2).[60,61] These results suggest that the functionalised magnetic PSSQ hybrids synthesised from the various surface functional groups can show excellent metal ions adsorption behaviour. Overall, these findings highlight the excellent adsorption and selectivity to Fe^{3+} and some heavy metals ions in the individual, mixed metal ions solutions, and artificial waste water. The dramatic advantages of these materials highlight the potential use for other applications.

Table 3 Comparison of Fe^{3+} adsorption on various materials

Sample name	Adsorption capacity (mg g^{-1})	Ref.
Acid activated montmorillonite	18.2	51
2-Vinylpyridine-divinylbenzene copolymer	28.50	52
Activated carbon based urea formaldehyde resin	29.66	53
Pentane-1,2-dicarboxylic acid functionalized spherical MCM-41	30.0	50
7-Amine-4-azaheptylsilica gel	39.65	54
10-Amine-4-azadecylsilica gel	57.22	54
Acryl amide/maleic acid hydrogel	42.30	55
Chitosan tripolyphosphate beads	53.9	56
Palygorskite nanoparticles	60.5	57
Kaolinite suspensions	65.0	58
Surface treated clinoptilolite	104.0	59
FeSo (Ind. Met)	68.4	This study
FeS1 (Ind. Met)	177.8	This study
FeS3 (Ind. Met)	164.8	This study
FeS0 (Mix. Met)	71.74	This study
FeS1 (Mix. Met)	177.9	This study
FeS3 (Mix. Met)	165.8	This study
FeS0 (Art. waste water)	155.3	This study
FeS1 (Art. waste water)	332.1	This study
FeS3 (Art. waste water)	309.6	This study

Conclusions

Multi-functional magnetic PSSQ hybrid nanoparticles were synthesised in a one-pot approach. The FTIR spectra and XRD patterns confirmed the stable magnetite structures present in the magnetic nanoparticles before and after capping the functional groups with various silane precursors. The HRSEM images suggest that the synthesised magnetite nanoparticles were spherical in shape with a uniform morphology. On the other hand, the functionalised magnetic PSSQ hybrid nanoparticles showed spherical magnetite nanoparticles covered with PSSQ networks. Furthermore, HR-TEM also confirmed the structural morphology of the samples. The nanoparticles showed good thermal stability and excellent magnetic behaviour with superparamagnetic properties. The functional magnetic nanoparticles showed excellent adsorption capacity (180–320 mg g^{-1}), removal efficiency (~90%), and selectivity (50–80%) to Fe^{3+} from the individual, mixed metal ions solutions, and artificial waste water. On the other hand, the adsorption behaviour of heavy metal ions were based on the types of surface functional groups present in the magnetic nanoparticles. The magnetic and functional magnetic nanoparticles can be separated easily from the adsorbed solution by a bar magnet and reused for the repeated cycles of adsorption. The recycling tests also suggest the excellent adsorption behaviour of functionalised magnetic nanoparticles for repeated use. The functional magnetic PSSQ hybrid nanoparticles can also be used for a range of applications due to the excellent properties, adsorption behaviour, and easily recyclable by an external magnet without the loss of samples. The easy synthesis, magnetic responsive adsorption behaviour, repeated usage for cycling test, and excellent adsorption behaviour of the functionalised PSSQ make these materials more useful for commercial applications.

Acknowledgements

The work was financially supported by the "2016 Post-Doc Development Program" of Pusan National University, Korea and the National Research Foundation of Korea (NRF) Grant funded by the Ministry of Science, ICT & Future Planning, Korea, Acceleration Research Program (NRF-2014R1A2A1A11054584) and Brain Korea 21 Plus Program (21A2013800002).

Notes and references

1 K. Vaaramaa and J. Lehto, *Desalination*, 2003, **155**, 157–170.
2 S. Nagappan, S. S. Park, P. K. Tapaswi, K. M. Rao, C. S. Ha and T. S. Hwang, *J. Porous Mater.*, 2015, **22**, 229–238.

3 M. S. Moorthy, M. J. Kim, J. H. Bae, S. S. Park, N. Saravanan, S. H. Kim and C. S. Ha, *Eur. J. Inorg. Chem.*, 2013, **17**, 3028–3038.
4 E. Swaminathan, S. Nagappan, P. Rajangam and S. Dharmalingam, *Progress in Nanotechnology and Nanomaterials*, 2013, **2**, 47–54.
5 S. Chaturvedi and P. N. Dave, *Desalination*, 2012, **303**, 1–11.
6 D. M. Vasudevan and S. Sreekumari, *Text book of biochemistry for medical students*, Jaypee Publication, New Delhi, 5th edn, 2007, pp. 76–91.
7 N. Abbaspour, R. Hurrell and R. Kelishadi, *J. Res. Med. Sci.*, 2014, **19**, 164–174.
8 P. T. Lieu, M. Heiskala, P. A. Peterson and Y. Yang, *Mol. Aspects Med.*, 2001, **22**, 1–87.
9 N. P. Arora and J. K. Ghali, *Heart Failure Rev.*, 2013, **18**, 485–501.
10 J. L. Sullivan, *Lancet*, 1981, **1**, 1293–1294.
11 J. L. Sullivan, *Exp. Biol. Med.*, 2007, **232**, 1014–1020.
12 V. P. Perez, M. N. M. de Lima, R. S. da Silva, A. S. Dornelles, G. Vedana, M. R. Bogo, C. D. Bonan and N. Schroler, *Curr. Neurovasc. Res.*, 2010, **7**, 15–22.
13 World Health Organization (WHO), *Guidelines for Drinking Water Quality, Recommendations*, WHO, Geneva, Switzerland, 1984, vol. 1, p. 79.
14 World Health Organization (WHO), *Iron deficiency anaemia: assessment, prevention and control: a guide for programme managers*, 2001.
15 S. W. Kuo and F. C. Chang, *Prog. Polym. Sci.*, 2011, **36**, 1649–1696.
16 (*a*) F. Dong, W. Guo, S. W. Chu and C. S. Ha, *Chem. Commun.*, 2010, **46**, 7498–7500; (*b*) F. Dong, W. Guo, S. S. Park and C. S. Ha, *J. Mater. Chem.*, 2011, **21**, 10744–10749; (*c*) F. Dong, W. Guo, J. H. Bae, S. H. Kim and C. S. Ha, *Chem.–Eur. J.*, 2011, **17**, 12802–12808; (*d*) F. Dong, W. Guo, S. S. Park and C. S. Ha, *Chem. Commun.*, 2012, **48**, 1108–1110.
17 M. C. Burleigh, S. Dai, E. W. Hagaman and J. S. Lin, *Chem. Mater.*, 2001, **13**, 2537–2546.
18 X. Duan, G. Qi, P. Wang and E. P. Giannelis, *ChemPhysChem*, 2012, **13**, 2536–2539.
19 X. Lu, Q. Yin, Z. Xin and Z. Zhang, *Chem. Eng. Sci.*, 2010, **65**, 6471–6477.
20 W. Wang, M. Chen, X. Chen and J. Wang, *Chem. Eng. J.*, 2014, **242**, 62–68.
21 R. G. Pearson, *J. Am. Chem. Soc.*, 1963, **85**, 3533–3539.
22 P. Figueira, C. B. Lopes, A. L. Daniel-da-Silva, E. Pereira, A. C. Duarte and T. Trindade, *Water Res.*, 2011, **45**, 5773–5784.
23 S. Nagappan, J. J. Park, S. S. Park, W. K. Lee and C. S. Ha, *J. Mater. Chem. A*, 2013, **1**, 6761–6769.
24 J. Liu, S. Z. Qiao, Q. H. Hu and G. Q. Lu, *Small*, 2011, **7**, 425–443.
25 L. H. Reddy, J. L. Arias, J. Nicolas and P. Couvreur, *Chem. Rev.*, 2012, **112**, 5818–5878.
26 S. Singamaneni, V. N. Bliznyuk, C. Binek and E. Y. Tsymbal, *J. Mater. Chem.*, 2011, **21**, 16819–16845.
27 S. Nagappan and C. S. Ha, *J. Mater. Chem. A*, 2015, **3**, 3224–3251.
28 J. H. Jung, J. H. Lee and S. Shinkai, *Chem. Soc. Rev.*, 2011, **40**, 4464–4474.
29 O. Hakami, Y. Zhang and C. J. Banks, *Water Res.*, 2012, **46**, 3913–3922.
30 H. Parham, B. Zargar and R. Shiralipour, *J. Hazard. Mater.*, 2012, **205–206**, 94–100.
31 E. Boyacı, A. Cağır, T. Shahwan and A. E. Eroğlu, *Talanta*, 2011, **85**, 1517–1525.
32 W. Wu, X. Xiao, S. Zhang, F. Ren and C. Jiang, *Nanoscale Res. Lett.*, 2011, **6**, 533.
33 L. Li, W. Jiang, K. Luo, H. Song, F. Lan, Y. Wu and Z. Gu, *Theranostics*, 2013, **3**, 595–615.
34 S. A. Corr, Y. P. Rakovich and Y. K. Gun'ko, *Nanoscale Res. Lett.*, 2008, **3**, 87–104.
35 A. K. Gupta and M. Gupta, *Biomaterials*, 2005, **26**, 3995–4021.
36 M. Zhang, G. Pan, D. Zhao and G. He, *Environ. Pollut.*, 2011, **159**, 3509–3514.
37 O. U. Rahman, S. C. Mohapatra and S. Ahmad, *Mater. Chem. Phys.*, 2012, **132**, 196–202.
38 Z. Salehi, H. H. Ghahfarokhi, A. A. kodadadi and R. Rahimnia, *J. Ind. Eng. Chem.*, 2016, **35**, 224–230.
39 S. Nagappan, S. S. Park, E. J. Yu, H. J. Cho, J. J. Park, W. K. Lee and C. S. Ha, *J. Mater. Chem. A*, 2013, **1**, 12144–12153.
40 L. Giraldo, A. Erto and J. C. Moreno-pirajan, *Adsorption*, 2013, **19**, 465–474.
41 Y. Wang, G. Morin, G. Ona-Nguema, F. Juillot, G. Calas and G. E. Brown, *Environ. Sci. Technol.*, 2011, **45**, 7258–7266.
42 S. R. Chowdhury and E. K. Yanful, *J. Environ. Manage.*, 2010, **91**, 2238–2247.
43 E. F. S. Vieira, J. A. Simoni and C. Airoldi, *J. Mater. Chem.*, 1997, **7**, 2249–2252.
44 A. M. Liu, K. Hidajat, S. Kawi and D. Y. Zhao, *Chem. Commun.*, 2000, 1145–1146.
45 W. Yantasee, C. L. Warner, T. Sangvanich, R. S. Addleman, T. G. Carter, R. J. Wiacek, G. E. Fryxell, C. Timchalk and M. G. Warner, *Environ. Sci. Technol.*, 2007, **41**, 5114–5119.
46 T. Sangvanich, J. Morry, C. Fox, W. Ngamcherdtrakul, S. Goodyear, D. Castro, G. E. Fryxell, R. S. Addleman, A. O. Summers and W. Yantasee, *ACS Appl. Mater. Interfaces*, 2014, **6**, 5483–5493.
47 J. Shi, H. Li, H. Lu and X. Zhao, *J. Chem. Eng. Data*, 2015, **60**, 2035–2041.
48 S. Hokkanen, E. Repo and M. Sillanpaa, *Chem. Eng. J.*, 2013, **223**, 40–47.
49 F. An, B. Gao, X. Dai, M. Wang and X. Wang, *J. Hazard. Mater.*, 2011, **192**, 956–962.
50 S. Parambadath, A. Mathew, S. S. Park and C. S. Ha, *J. Environ. Chem. Eng.*, 2015, **3**, 1918–1927.
51 K. G. Bhattacharyya and S. S. Gupta, *Adsorption*, 2006, **12**, 185–204.
52 D. Rabelo, V. J. Silva, E. F. C. Alcantara, L. C. Faria, G. A. V. Martins, V. K. Garg, A. C. Oliveira and P. C. Morais, *J. Appl. Polym. Sci.*, 2003, **89**, 3905–3912.
53 O. G. Li, G. J. Feng, H. T. Ping, A. F. Qiang, W. Yu, W. Y. Jun and Z. Dong, *RSC Adv.*, 2015, **5**, 71878–71882.

54 C. G. Passos, F. S. Ribaski, N. M. Simon, A. A. dos Santos Jr, J. C. P. Vaghetti, E. V. Benvenutti and É. C. Lima, *J. Colloid Interface Sci.*, 2006, **302**, 396–407.
55 D. Saraydin, E. Karadag and O. Guven, *Sep. Sci. Technol.*, 1995, **30**, 3287–3298.
56 Z. Yalinca, E. Yilmaz and F. T. Bullici, *J. Appl. Polym. Sci.*, 2012, **125**, 1493–1505.
57 A. Middea, T. L. A. P. Fernandes, R. Neumann, O. D. F. M. Gomes and L. S. Spinelli, *Appl. Surf. Sci.*, 2013, **282**, 253–258.
58 K. Ma and A. C. Pierre, *Clays Clay Miner.*, 1997, **45**, 733–744.
59 N. A. Oztas, A. Karabakan and O. Topal, *Microporous Mesoporous Mater.*, 2008, **111**, 200–205.
60 V. K. Gupta and A. Nayak, *Chem. Eng. J.*, 2012, **180**, 81–90.
61 Y. S. Ho and G. McKay, *Process Biochem.*, 1999, **34**, 451–465.